CHALMERS | UNIVERSITY OF GOTHENBURG

Calibration detector for Crystal Ball

Thomas Axelsson
Vedad Babic
Per M Hansson
Johannes Laurell Håkansson
Nikita S Kudelkin
Niklas Rosholm

Supervisor:
Andreas Heinz
Co-Supervisor:
Håkan Johansson

Department of Fundamental physics
Division of Subatomic physics
Chalmers University of Technology
University of Gothenburg
Gothenburg, Sweden 2012

Bachelor's project FUFX02-12-02

Abstract

Crystal Ball is a detector which can be used for detection of high energy protons, but this task requires a potentially tedious and expensive task of calibrating it. In this study, a test setup using a single NaI crystal from the Crystal Ball was considered to investigate the possibility of using cosmic muons to calibrate the Crystal Ball. The study was performed by simulating the process using the Geant4 toolkit. A program was written to simulate the passage of cosmic muons and protons through the Crystal Ball crystal, record the deposited energy and correlate these to each other. A setup which can be used for finding the correlation experimentally is proposed. Using the results from the experiment, it is possible to calibrate all crystals in Crystal Ball using cosmic muons.

Contents

1 Introduction

1.1 Background

The goal of research within the field of subatomic physics is to gain knowledge about the properties and structure of nuclei. This is done through experiments where results from collisions between particles are analyzed.

GSI in Darmstadt, Germany, is one site where this area of physics is explored. This research is conducted using equipment consisting of particle accelerators, detectors etc. One piece of equipment, which is the focus of this project, is the Crystal Ball.

Crystal Ball is a detector array which serves as a 4-π-spectrometer and consists of 162 NaI crystals put closely together to form a sphere with an inner radius of 25 cm and an outer radius of 45 cm (see Figure 1).

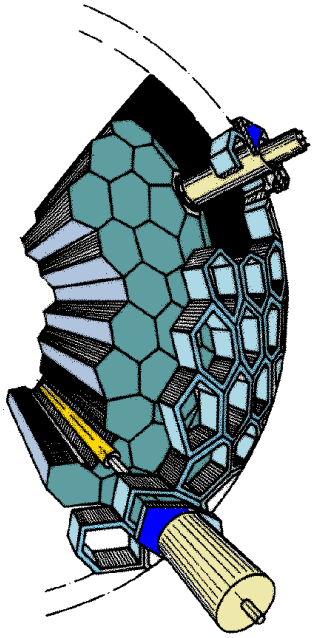

Figure 1: A closer look at a section of the Crystal Ball's detector array [1].

When conducting an experiment, one places a target in the centre of the Crystal Ball. This target can be, for example, made of plastic, carbon or lead. A beam of unstable particles, which are created in a nuclear reactions at a production target, collides with the experimental target nuclei. Due to kinematics most reaction products move in the forward direction but some of the lighter particles scatter at larger angles. To detect these particles and photons, Crystal Ball is used.

Being initially optimized for detection of low energy γ-rays ($1 - 3$ MeV), the Crystal Ball is now also used for detection of high energy protons (several hundred MeV). To make a good use of it for detection of high-energy protons it needs a proper calibration.

A problem arises in the question of how to calibrate all detectors of Crystal Ball. Since it is

both expensive and burdensome to calibrate all crystals one by one with a proton beam, there is a need of a freely available source with a well-defined energy spectrum to be used for calibration. A candidate for such a source are cosmic muons. These particles are created in the atmosphere as a result of a cascade of reactions that follow from the interaction of cosmic radiation with the nuclei of air molecules, see Section 2.3 for more information.

To make use of the muons, it is sufficient to calibrate one crystal with the proton beam and correlate this to the energy deposit in the crystal from the muons. This can be done because the energy spectrum of the muons and their angular distribution are well known [12]. This way they can be used to calibrate the other crystals for detection of high energy protons.

Since the energy deposited by muons depends on the length traversed through crystal, it is desirable to track the path through the crystal taken by the muons. In the Crystal Ball, several crystals fire off when a particle passes through them, enabling path tracking. For a single crystal there will not be any crystals nearby to fill this role. Therefore one uses plastic scintillators, which are cheap and easy to handle, to track the path length. See Section 2.1 for more information on scintillators.

1.2 Purpose and objectives

The purpose of the project is to develop a way of calibrating a Crystal Ball crystal with cosmic muons. This is done by selecting a suitable detector setup for calibration of a single Crystal Ball crystal against protons which in turn is to be used to calibrate all detectors of Christal Ball with muons on the basis of Monte Carlo simulations.

The experiment was not executed within this project. The purpose of the project is to provide simulations and guidelines for an upcoming experiment.

2 Theory

2.1 Scintillators

A scintillator is a material that de-excites by emission of light when atoms in it have been excited by ionizing radiation, a luminescence process called scintillation. There are a lot of different types of scintillators with different properties but the only ones relevant for this work are plastic scintillators and sodium iodide crystals of Crystal Ball which are doped with thallium (Tl).

Sodium iodide is used as a scintillator material because of its good stopping power and energy resolution [6]. The resolution for stopped protons in a NaI crystal is 2% or less. For punchthrough protons the resolution is around 5% [**?**]. The reason for using plastic scintillators is for convenience as plastic is cheap, easy to manufacture, shape and handle. Moreover, plastic scintillators give a very fast response [6].

2.1.1 Inorganic scintillators

In a crystal of sodium iodide (NaI), which is an inorganic material, the scintillation occurs due to the crystal structure of the lattice. It has a large energy band-gap from the valence to the conduction band making photon emission an inefficient way of de-excitation of the material. Due

to this fact one adds an activator (in our case thallium), an impurity, to the crystal to add extra energy-bands in the forbidden zone between valence and conduction band. The activator is added in trace amounts, meaning that the overall energy structure of the crystal remains unchanged, while the band structure at the lattice point where the activator is being placed, is changed. The activator is chosen such that it allows photons with lower energies, lying in the visible range of light, to be emitted with higher probability.

2.1.2 Organic scintillators

In contrast to inorganic scintillators, the scintillation of organic scintillators does not appear due to the lattice structure of a crystal, but rather it originates from the fluorescence mechanism of single molecules. The fluorescence arises from transitions in the energy levels of these molecules and is independent of the state in which the molecules are in, be it a gaseous mix or a solid.

2.1.3 Measurements and Equipment

To make use of a scintillator one needs to connect photomultiplier tubes (PMTs) to it. These together with some electronic equipment constitute a scintillation counter. This makes it possible to detect the scintillation photons, which are in turn transformed into an electric signal with a certain amplitude.

2.2 Minimum ionizing particles

Energy loss in a material can be of different types, such as ionization, radiative processes and others. Which of these processes that dominate the total energy loss depends on the energy of the incoming particle as well as the material used. If the energy of the incoming particle is within a specific interval of energy the energy loss per unit path length goes to a minimum. These particles are called minimum ionizing particles [8].

At energies up to about 100 GeV, the deposited energy in the crystal is described by the Bethe-Bloch formula [10].

At energies well above 100 GeV radiative processes will become the main factor for determining deposited energy, as opposed to ionization. Cosmic muons have energies well within the range where muons can be treated as minimum ionizing particles [9]. In Figure 2 one can see an example of what the region of minimum ionization for muons looks like.

A minimum ionizing particle's energy loss in a material is only dependent on the thickness of the material passed. The stopping power in the region $0.1 - 50\,\mathrm{GeV}$ varies very weakly with the energy of the muons ($1.5 - 2.1\,\frac{\mathrm{MeVcm}^2}{\mathrm{g}}$) (see Figure 2). Therefore a broad energy distribution may result in a well-defined energy deposit in a detector. Hence it can be used for calibration.

2.3 Muons

A muon is an unstable subatomic particle with a charge equal to that of an electron and a mass of $105.7\,\mathrm{MeV/c^2}$, which corresponds to 206.8 times the mass of an electron [7]. Most muons on earth are created in the upper atmosphere, usually through the process described below.

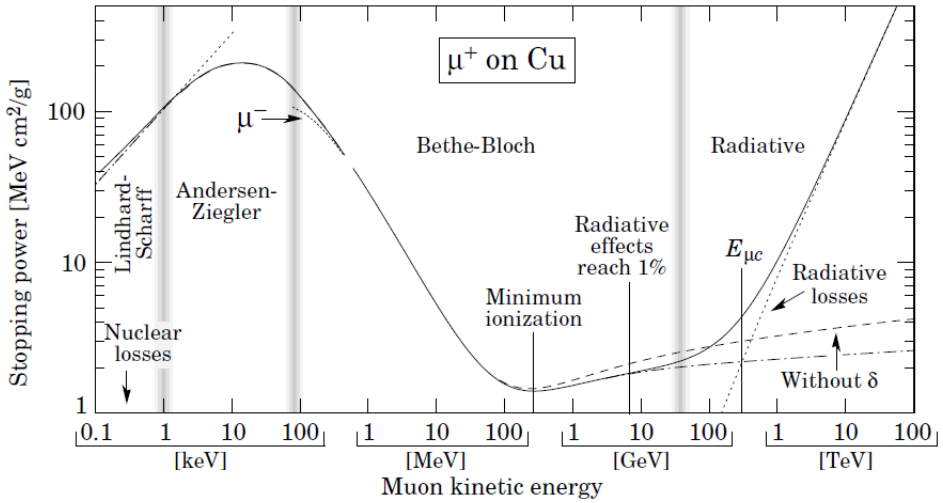

Figure 2: Stopping power for μ^+ in Cu as a function of the kinetic energy of the muon [10]

.

As high-energy nuclei from cosmic rays interact with atmospheric nuclei, kaons and pions are produced. A negative pion decays to a muon and a muon-type antineutrino, with a mean lifetime of about 26 ns, and thus survives only a few meters on average. The muon created has a mean lifetime of 2.2 μs and decays to an electron, an electron-type antineutrino and a muon-type neutrino. The different reactions and decays are shown in (1).

$$\begin{aligned} A_{cr} + A_{air} &\rightarrow \pi^{\pm}, K^{\pm}, K^0 \\ \pi^- &\rightarrow \mu^- + \bar{\nu}_\mu \\ \mu^- &\rightarrow e^- + \bar{\nu}_e + \nu_\mu \end{aligned} \tag{1}$$

The somewhat longer half-life of the muon is due to the fact that it decays by the weak force. The time dilation effect of special relativity results in a mean traveled distance that is sufficiently large that about 10 % of the muons reach sea level [14]. The muons travel generally in the same direction as the cosmic rays from which they originate.

The intensity of incoming muons at sea level depends on the incident zenith angle as well as muon energy and this dependence has been measured. It is described by equation (2), where p_μ is the muon momentum in GeV/c, $I(0)$ is the vertical intensity and θ is the zenith angle [13].

$$\log(I(\theta)) = a \ln^2 p_\mu + b \ln p_\mu + c \tag{2}$$

Equation (3) below is used to obtain the parameters a, b and c, using data from Table 1. These relations describe the measured intensities for muons with an energy between $0.2 - 100$ GeV/c [13], which corresponds to the energy region where muons can be treated as minimum ionizing particles [9].

$$Y = p_1/(1/\theta + p_2\theta) + p_3 + p_4 \exp(-p_5\theta) \tag{3}$$

Table 1: Parameters for the equations (2) and (3) [12].

	a	b	c
p_1	$-0.8816 \cdot 10^{-4}$	$+0.4169 \cdot 10^{-2}$	$-0.3516 \cdot 10^{-3}$
p_2	$-0.1117 \cdot 10^{-3}$	$-0.9891 \cdot 10^{-4}$	$+0.8861 \cdot 10^{-2}$
p_3	-0.1096	$+4.0395$	-2.5985
p_4	$-0.1966 \cdot 10^{-1}$	-4.3118	$-0.8745 \cdot 10^{-5}$
p_5	$+0.2040 \cdot 10^{-1}$	$-0.9235 \cdot 10^{-3}$	-0.1457

2.4 Punchthrough of particles

The Crystal Ball crystals, initially not designed for detection of high energy protons, are not long enough to stop all the protons liberated liberated in the exeriments during their path in the crystal.

Punchthrough describes the situation of a particle traveling through a material, ionizing it and losing only a part of its kinetic energy. If the particle does not lose all of its kinetic energy, it will continue its path out of the material and thus 'punch through' the material, see the upper part of Figure 3.

The opposite process is total loss of kinetic energy, resulting in the incoming particle being stopped in the material. The particle never escapes the boundaries of the material as seen in the lower part of Figure 3.

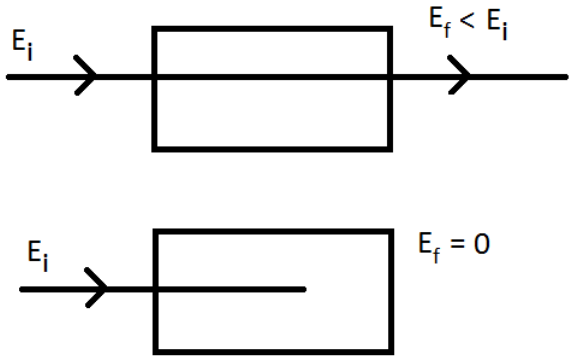

Figure 3: The upper figure demonstrates punchthrough while the lower figure demonstrates a particle being stopped. The initial and final energies, E_i and E_f, are the kinetic energies of the particles.

3 Method

3.1 Geant4

The test setup consists of one Crystal Ball detector and plastic scintillators. The latter are necessary to determine the trajectories of incoming muons. In the present study, simulations

were conducted with version 9.4 of the Geant4 toolkit. Geant4 is an object oriented development framework developed at CERN (the European Organization for Nuclear Research) for "simulating the passage of particles through matter", and was developed for making accurate simulations of particle detectors, but has many applications in e.g. medicine and astrophysics [2]. The toolkit, based on the programming language C++, allows the user to define the geometry of a detector with different materials, and then simulate particles and track their interactions with the detector through a cornucopia of physics processes.

The Geant4 framework handles runs, events and the tracking of particles, all of which are available for the user to manipulate. Here, a run is a preset number of particles to be generated in the simulation, an event is the simulation of a single particle. The tracking of a particle is handled in small steps, as it traverses the materials in the detector. The programmer can supply his own code to conduct a virtual experiment - from the geometry and materials in the detector, to the number of simulated particles and particle direction. There is also a possibility to manipulate data output after need[3].

Geant4 simulates electromagnetic processes, as well as hadronic interactions for high- and low-energy physics and uses Monte Carlo methods for calculating the probability of certain events occurring, see Table 2. The Monte Carlo engine of Geant4 handles probabilities for the occurance of physics processes and, as is the case with all statistical processes, an error results from such simulations. The validity and accuracy of Geant4 simulations of electromagnetic processes has been proven in a number of studies [5], [4].

3.2 Software for simulations

To study basic physics processes with muons and protons in a scintillating material, a program was written within the Geant4 framework that generated particles of a user defined energy with momentum along the symmetry axis of a cylinder with length 20.0 cm and diameter 10.0 cm. See Figure 4 for an example of the visual output from the program.

To run simulations of an actual crystal from the Crystal Ball array together with plastic scintillators, another program was written that reads a scintillator setup from a user created data file. This program also employs a realistic angle- and energy distribution of muons, together with the geometry of a Crystal Ball crystal. All scintillators were simulated as having a thickness of 0.5 cm.

The Crystal Ball is made up of crystals of four different crystal shapes in order to build up a solid, hollow sphere, much like the pattern of hexagons and pentagons on a soccer ball. The measures for the crystal were obtained from GSI, and the shape called "D" is expected to be used for the calibration experiment. The crystal is defined by the points (6.8, 4.3305), (0.0, 10.08625), (-6.8, 4.3305), (-6.8, -4.3305), (0.0, -10.08625), (6.8, -4.3305) all measures in cm taken at a reference radius of 49.86932985 cm, see Figure 5. The shape is then spanned between an inner radius of 25 cm and an outer radius of 45 cm. See Figure 6 for an example of visual output from the program and illustration of the crystal shape.

For every event the program saves the amount of energy that is deposited in the crystal, and in the scintillators, to enable a post hoc coincidence measurement. Data was collected and analyzed with the ROOT toolkit [18].

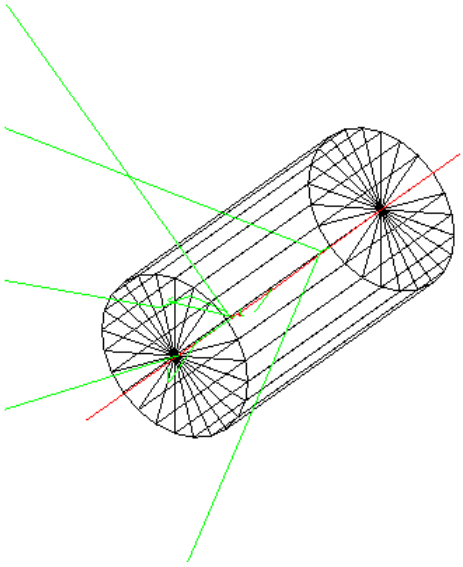

Figure 4: Visual output from the experimental setup in Geant4 - a muon (red line) passing through a NaI crystal. The green lines are gamma photons.

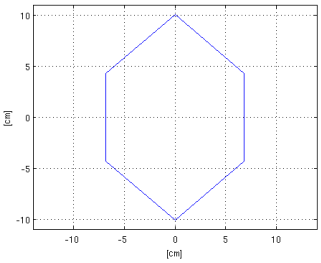

Figure 5: Profile of crystal shape ''D" used in simulations.

3.3 Simulated materials and processes

For the NaI Crystal data from Geant4's included NIST material database was used, while the material in the plastic scintillators were defined as polyvinyl toulene, a common material for plastic scintillators. The material was defined in Geant4 as a mix of H and C with a total density of $1.032\,\mathrm{g/cm^3}$, and a ratio between H/C of 10/9 [19]. The physics processes included in the simulations can be found in Table 2.

3.4 Simulations of horizontal scintillators

In order to investigate how scintillator size and separation might affect measurement accuracy and measurement time for horizontal muons, a set of scintillator setups was created (see Figure 7). The muon flux is at its lowest at the horizontal, so it was decided that the scintillator at the narrow (front) end of the crystal should be made as large as the geometry allowed for, and this

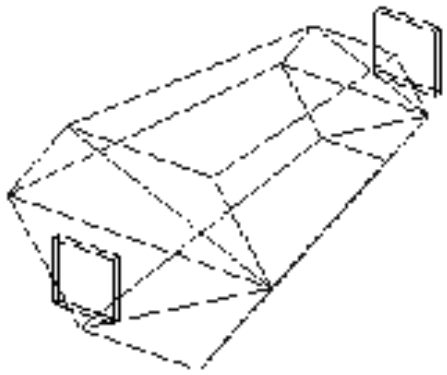

Figure 6: Visual output from the experimental setup in Geant4 - a crystal together with two plastic scintillators.

Table 2: Table of particles and associated physics processes included in the simulations.

Particle	Enabled processes
Gamma photons	
	Photoelectric effect
	Compton scattering
	Gamma conversion
Electrons/Protons	
	Multiple scattering
	Ionisation
	Bremsstrahlung
	Pair production
Muons	
	Multiple scattering
	Ionisation
	Bremsstrahlung
Protons	
	Multiple scattering
	Ionisation
	Bremsstrahlung
	Pair production
Alpha/He-3/Ions	
	Multiple scattering
	Ionisation

size was kept at a constant 5.5×5.5 cm. The scintillator at the broader (back) end of the crystal was changed in size, and the sizes 5.5×5.5 cm, 9.5×9.5 cm, 13.5×13.5 cm and 17.5×17.5 cm were tested.

After initial analysis of the data it was decided to run further simulations on a scintillator setup with a more favorable geometry. The scintillator at the narrow (front) end of the crystal was chosen with a size of 5×5 cm and the scintillator at the broader (back) end of the crystal with a size of 13.7×13.7 cm.

In order to investigate how the separation between the front- and back scintillators affected measurements, simulations were run where the scintillators' areas were kept constant at 5×5 cm, while their separation was changed to 42 cm, 47 cm, 52 cm and 57 cm. See Figure 7 for a schematic view of the changes in separation and size. The back scintillators were placed with a distance of at least 0.5 cm from the simulated equipment, and with enough space to fit a PMT between one scintillator and the crystal.

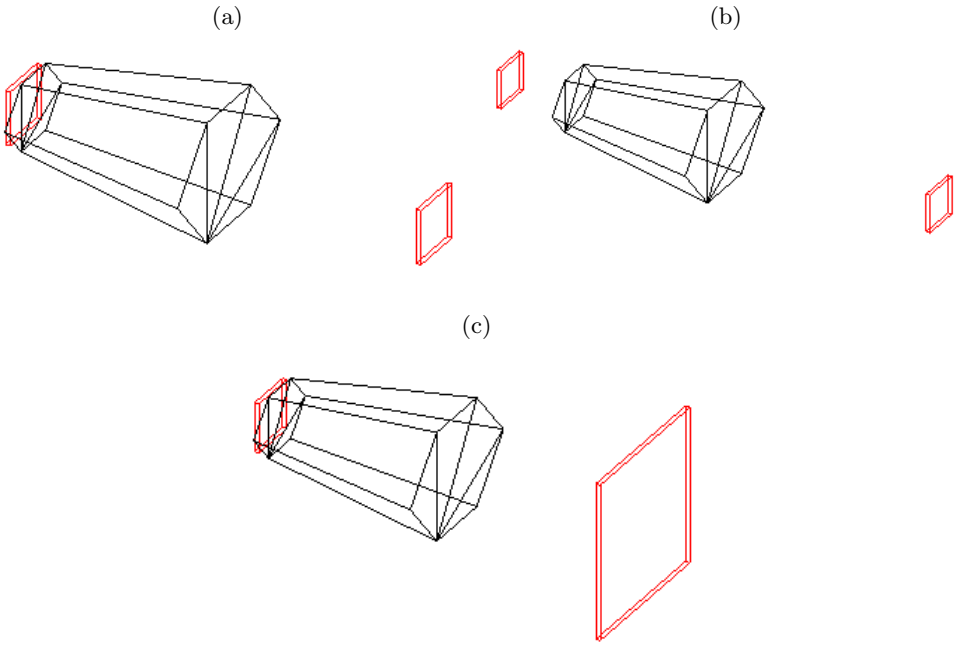

Figure 7: Extremes for scintillator size and placement in the simulations of horizontal detection: (a) closest to crystal and PM-tube, (b) furthest apart, (c) largest tested back scintillator.

To cut down simulation time the simulations were run with a modified muon distribution that only simulated particles coming from zenith angle between 60° and 90°, i.e. candidates for actually traversing both scintillators.

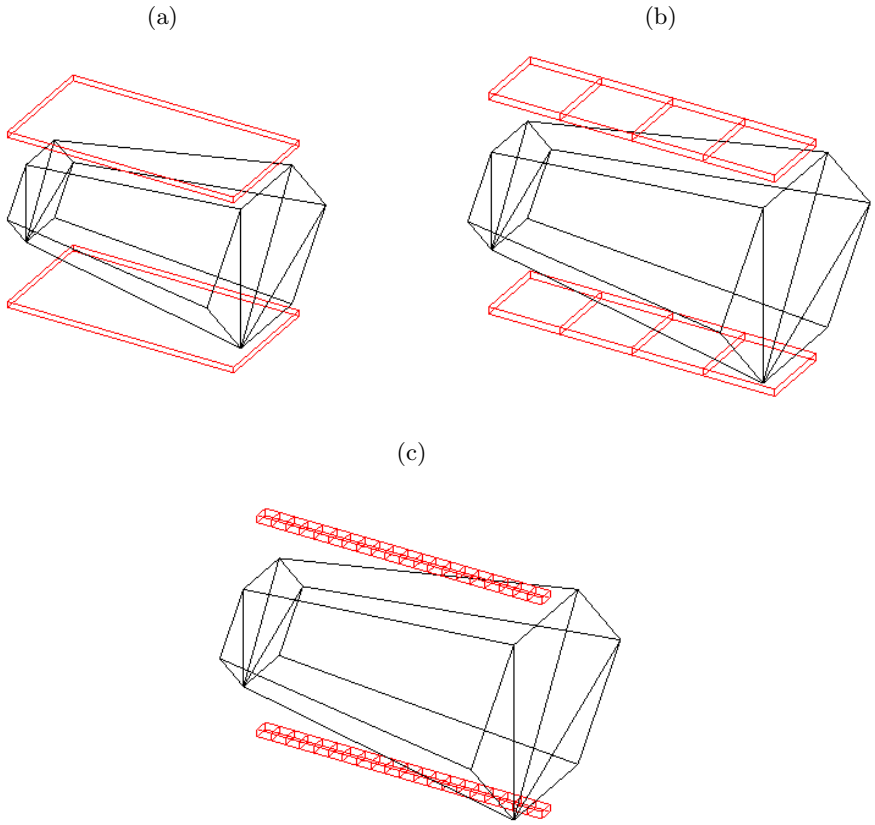

Figure 8: Some of the different setups used to detect vertical muons: two rows of (a) one $10 \times 20\,\mathrm{cm}$ scintillator, (b) four $5 \times 5\,\mathrm{cm}$ scintillators, (c) twenty $1 \times 1\,\mathrm{cm}$ scintillators.

3.5 Simulations of vertical scintillators

3.6 Theoretical muon particle flux through a simple scintillator setup

The angular intensity of cosmic muons can be approximated using the following empirical relationship

$$I(\theta) \approx I(0)\cos^2\theta \tag{4}$$

where θ is the zenith angle and $I(0)$ the vertical intensity ($\theta = 0$) [13]. $I(\theta)$ is given in units of $\mathrm{cm}^{-2}\mathrm{s}^{-1}\mathrm{sr}^{-1}$, which means that $I(\theta)$ is the number of particles passing through a certain area from a certain solid angle every second. The angular intensity is uniform with respect to ϕ.

To calculate the muon particle flux, J, through a scintillator one needs to integrate the angular intensity over the solid angle Ω, which the scintillator sees.

$$J = \int I(\theta)\cos(\theta)\,\mathrm{d}\Omega \tag{5}$$

where the $\cos\theta$ term is due to the fact that the flux across a surface depends on the angle

between the surface normal and the direction of the particles.

The vertical intensity $I(0)$ is calculated by using equation (2) and integrating the expression for $I(0)$ with respect to the momentum, $1\,\mathrm{GeV/c} \leq p_\mu \leq 30\,\mathrm{GeV/c}$. Integration using MATLAB yields

$$\int_1^{30} I(0)\,\mathrm{d}p_\mu \approx 6.4 \cdot 10^{-3} cm^{-2} s^{-1} sr^{-1} \tag{6}$$

For a simple setup two square scintillators, of the same size, are placed one above the other at a certain distance from each other. The muon particle flux through this setup is equal to the flux through the bottom scintillator over the solid angle the bottom scintillator sees. To simplify the geometry the following two assumptions are made:

1. Each small area element of the scintillator sees the same solid angle as the one seen by the center of the detector.
2. The square scintillators are modeled as circular, having the same area.

The solid angle the bottom scintillator sees is now simply the solid angle subtended by a cone, see Figure 9.

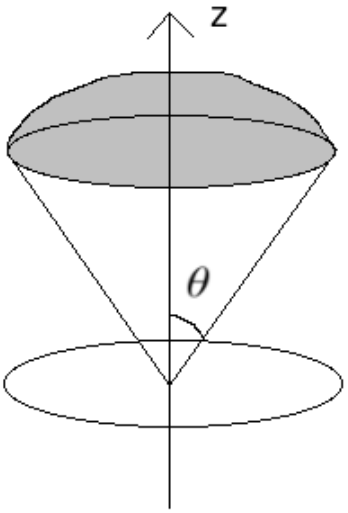

Figure 9: Explanatory sketch showing the solid angle seen by the center of the bottom scintillator.

$$\int_{cone} \mathrm{d}\Omega = \int_0^{\theta} \sin(\theta')\,\mathrm{d}\theta' \int_0^{2\pi} \mathrm{d}\phi \tag{7}$$

Combining equations (4), (5) and (7) yields a muon particle flux for this particular setup of

$$J \approx 2\pi \int_0^{\theta} (I(0)\cos^2\theta)\cos\theta\sin\theta\,\mathrm{d}\theta = \left(\frac{\pi}{2}\right) I(0)(1-\cos^4\theta) \tag{8}$$

where J is given in units of $\mathrm{cm}^{-2}\mathrm{s}^{-1}$. To get total number of muons that passes through the scintillator every second one simply multiplies J by the area

For a simple setup using square scintillators with a side length of 5 cm and a distance between the two of 41 cm equation (8) yields an estimated total muon particle flux, $J_tot = 0.0024\,\mathrm{s}^{-1}$ i.e. one muon passes the two detectors every 423 seconds ($\tau = 423\,\mathrm{s}$).

3.7 Muon particle flux through simulated detector configurations

As there is a finite time in which to perform the calibration with the single detector and its associated plastic scintillators, an estimation of the muon particle flux through different scintillator configurations is needed. A certain setup might give a well-defined path length through the crystal. If the number of muons that pass through that configuration of scintillators is very low though, the time required to get enough muons for good statistics is impractical.

To estimate the muon particle flux through different scintillator configurations the theoretical flux through a simple scintillator setup was calculated, see subsection 3.6. Simulations were then run on that setup and the number of hits were compared with the theoretical value, which resulted in a correlation factor between the two.

For the simulation mentioned above, a total of $6 \cdot 10^7$ particles were shot, 6476 of them passing the two vertically placed detectors. With a calculated theoretical value, τ, of one muon passing the vertical setup every 423 seconds, the simulation represented the setup being bombarbed by muons for a duration of $\tau \cdot 6476 \approx 2.74 \cdot 10^6\,\mathrm{s}$.

Also included in the same simulation were another pair of scintillators, these ones horizontally placed. This was done in order to correlate the ordinary muon distribution with the modified distribution mentioned in subsection 3.4. The scintillator setup used in the simulation is shown in Figure 10.

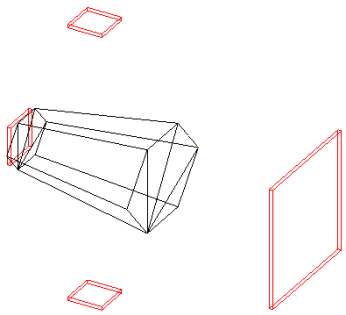

Figure 10: Setup used to obtain correlation factors between the real muon particle flux and the simulated.

3.8 Background

3.9 Distribution

In order to achieve a uniform distribution of muons impinging on the crystal a modified hemisphere was constructed around the crystal. Initially a position vector was randomized on the hemisphere with center in the origin, using uniformly randomized values of θ and ϕ in spherical coordinates.

$$\theta \epsilon [0, \frac{\pi}{2}] \tag{9}$$

$$\phi \epsilon [0, 2\pi] \tag{10}$$

This resulted in a position vector $\overrightarrow{v_p} = (x_p,y_p,z_p)$ with x_p, y_p and z_p given by equations (11)-(13), where R is the radius of the hemisphere.

$$x_p = R\cos\phi\sin\theta \tag{11}$$

$$y_p = R\sin\phi\sin\theta \tag{12}$$

$$z_p = R\cos\theta \tag{13}$$

An offset vector, $\overrightarrow{v_o}$, orthogonal to the position vector was obtained by deriving its coordinates with respect to θ. $\frac{\delta\overrightarrow{v_p}}{\delta\theta}$ was used since $\frac{\delta\overrightarrow{v_p}}{\delta\phi}$ is equal to zero at $\theta = 0$, and, thus, does not give us a uniform distribution.

The acquired offset vector was rotated by a randomized angle α around the position vector and its magnitude, r, was set by the the magnitude of the position vector times the square root of a randomized scalar between zero and one. This was done to achieve equal probability for each point on a disc tangential to the hemisphere.

$$m \epsilon [0, 1] \tag{14}$$

$$r = R\sqrt{m} \tag{15}$$

$$\alpha \epsilon [0, 2\pi] \tag{16}$$

The start position of the muon was set according to (17) (see Figure 11) and the momentum direction of the muon was set to $-\overrightarrow{v_p}$.

$$\overrightarrow{v} = \overrightarrow{v_p} + \overrightarrow{v_o} \tag{17}$$

The modified hemisphere was tested to make sure that it provides a uniform distribution. This was done by placing ten detectors at the bottom of the half sphere as rings at different radii but all of which had the same surface area on the top. Simulations were made where the number of hits on each surface were acquired. In table 3 the number of hits on each surface are given for a simulation of one million muons sent from the half sphere.

The distribution given by equation (2) was then implemented into the sphere. This was done by first randomizing values for θ and muon momentum in intervals appropriate for the

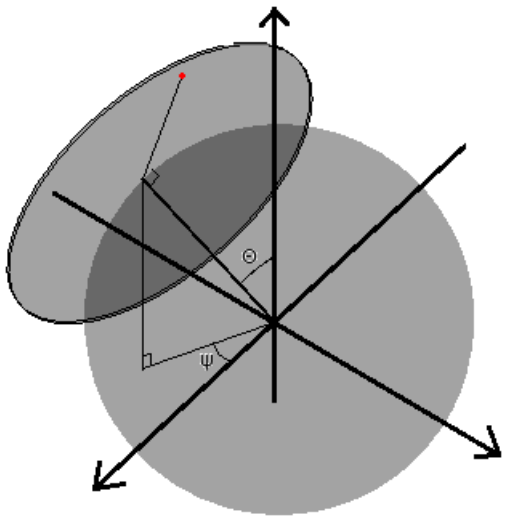

Figure 11: Visualisation of the modified hemisphere.

simulation, and using these values to calculate I as in equation (2). The result is then compared to a randomized test value between zero and the maximum value of I, and the particle is created if the test value was smaller than the value of I. If the test value is greater than I, then the values for θ, muon momentum and the test value are randomized again and the check redone. The cycle is repeated until the test value is smaller than I. This gives a proper setup for doing the simulations with the actual muon distribution. The distribution, as intensity plotted against zenith angle and muon momentum, is given in Figure 12.

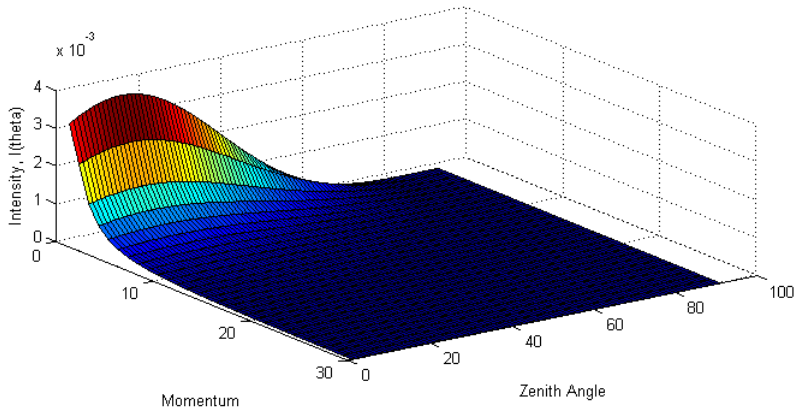

Figure 12: The muon distribution. Intensity of muons as a function of zenith angle (in °) and muon momentum (in GeV/c).

Hits per detector	
Detector 1	98860
Detector 2	100101
Detector 3	100280
Detector 4	99364
Detector 5	100284
Detector 6	100373
Detector 7	100421
Detector 8	100094
Detector 9	99922
Detector 10	100301

Table 3: Number of hits on each detector for 1 000 000 events from the half sphere for uniform distribution.

4 Calibration

All simulations were run with a NaI-cylinder crystal with a radius of 10 cm, the length was varied between 5 cm, 10 cm, 15 cm and 20 cm. The number of particles impinging was 10000 in all simulations. The incoming particles hit the crystal top surface perpendicular to it.

4.1 Muon behaviour

By impinging mono-energetic beams of muons into cylinders of fixed length one can find systematics in the deposited energy of the muons by varying these parameters. The deposited energy spectra that resulted from the simulation are fitted with Landau distributions. The fit includes three different parameters, one of which is the most interesting. This is the most probable value (MPV) which gives the most probable energy the muons deposit, along with its error.

4.1.1 Energy and length dependence

By collecting the information for different lengths traveled through the crystal at different energies one finds a relation between the two. The results are plotted in Figure 14. Since muons in this case are minimum ionizing particles, see section 2.2, it is expected that their energy deposit is linearly dependent on the traversed length through the crystal.

To find the dependence of incoming energy to deposited energy, muons traversing the crystal with energies varying from 0.5 GeV up to 20 GeV were simulated. This is confirmed by the results of our simulation presented in Figure 14. One can clearly see that the energy deposited does not vary much with incoming energy between 4 GeV and 20 GeV ($3.6\% - 4.15\%$ relative backward error). Once again this is due to the particles being minimum ionizing.

4.1.2 Surface effects

There exist surface effects i.e. the deposited energy varies depending on where the muon hits the crystal, that is, if it is close to the surface or not. One can argue that, as the muons impinge

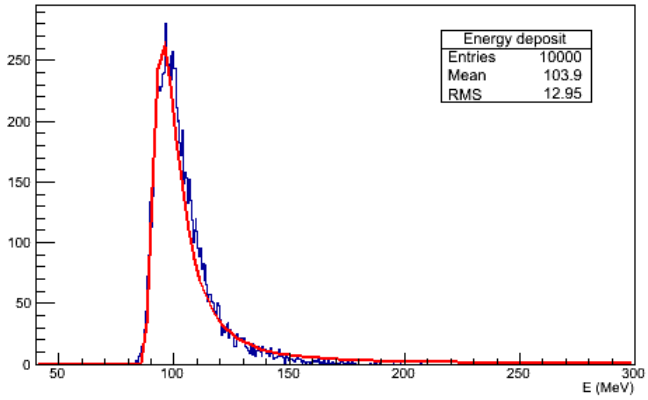

Figure 13: A Landau distribution fitted to data corresponding to the deposited energy of monoenergetic and monodirectional muons traversing a NaI-cylinder of length 20 cm. The muons have an kinetic energy of 1.0 GeV and traversed through the center of the cylinder. The variance is 12.272 MeV^2.

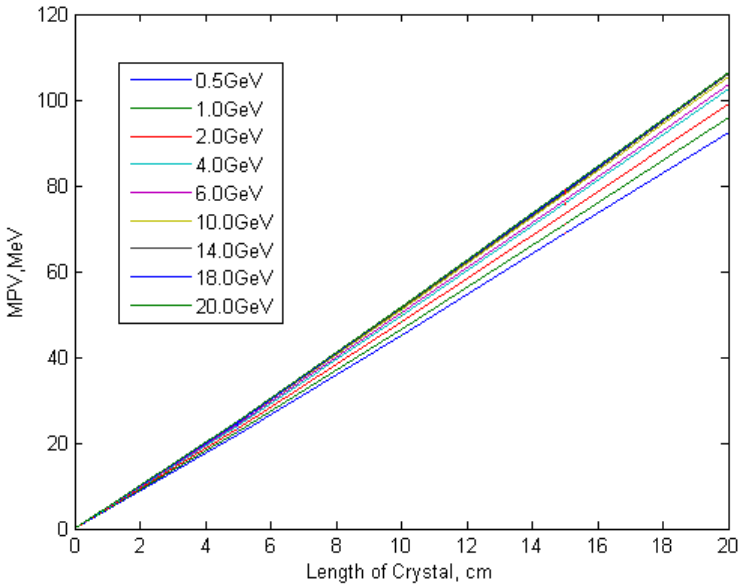

Figure 14: The most probable value (MPV) of deposited energy extracted from simulations where muons traversed the center of a NaI cylinder of varying length plotted against the cylinder length for different energies. The data is fitted to a landau distribution, see Figure 13. The graph includes error-bars from the fit of the MPV, although too small to be seen by the naked eye.

closer to the surface the secondary particles created can scatter out of the cylinder, which is demonstrated in Figure 16.

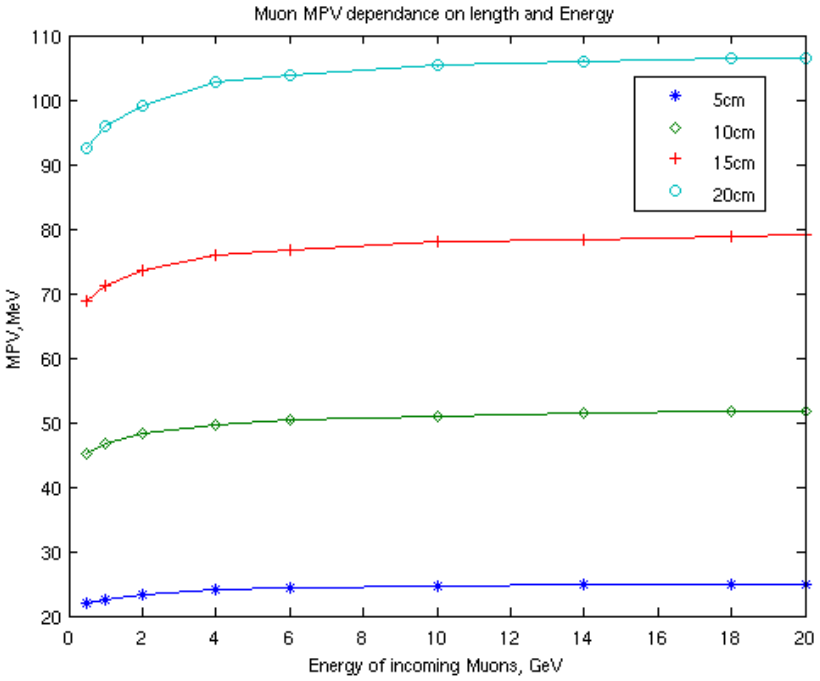

Figure 15: MPV from the Landau fit of energy deposited by muons with varying incoming energies. This was done for muons traversing four different lengths of an NaI crystal.

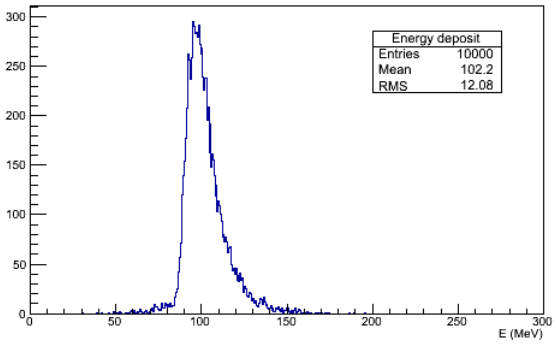

Figure 16: Deposited energy for muons hitting the NaI cylinder 0.9 cm from the edge. The cylinder's length is 20 cm.

In the region $50-70$ MeV there occured deposit of some lower energies which did not occur in Figure 13 where the muons hit the centre of the cylinder. As the beam gets closer to the surface, more precisely 0.03 cm from the side of the crystal there exists almost two equivalent peaks (see Figure 17). An examination of how the mean energy varies with distance to the surface was conducted, with results in Figure 18.

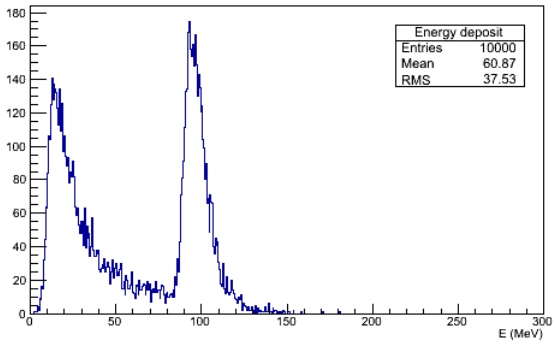

Figure 17: Energy deposited by muons impinging 0.03 cm from the surface of a 20 cm long NaI cylinder.

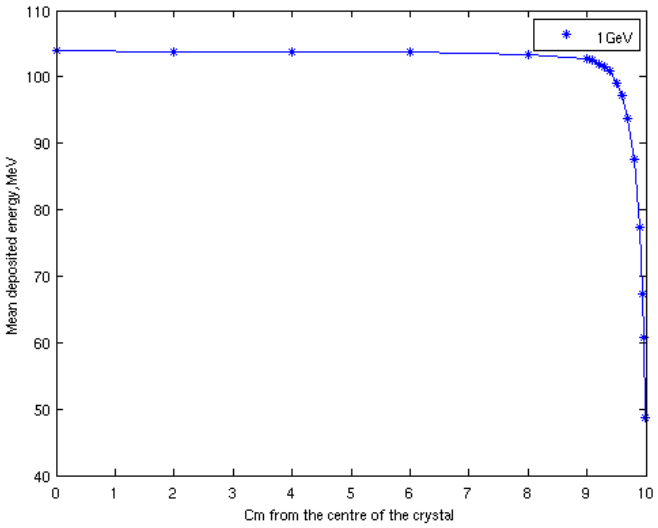

Figure 18: Surface effect illustrated by plotting the mean deposited energy of incoming muons with 1.0 GeV energy versus the distance from the centre where the muon hits the cylinder surface.

As seen in Figure 18 the effect occurs only when the particles get very close to the surface of the crystal. Therefore one should, when calibrating the crystal, position the scintillators in such a manner that trajectories of muons with less than 5 mm to the surface are suppressed.

4.2 Proton behaviour

Protons are, unlike muons, not minimum ionizing particles in the interesting energy range. Therefore one can not expect the energy deposit to behave like the energy loss experienced by muons. The histograms that result from the proton simulations were fitted with Gaussian distributions instead of Landau distributions used for muons. For sub-punchthrough energies, the histograms

were not fitted with any function since the protons deposit all their energy and give rise to a well-defined peak, see Figure 19.

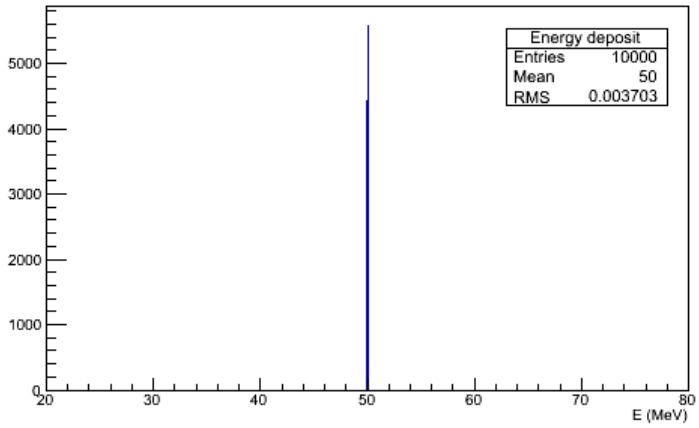

Figure 19: The energy deposited by protons with 50 MeV kinetic energy in a 10 cm long NaI crystal. The variance, resulting from a Gaussian fit, is 0.172215 MeV^2.

4.2.1 Punchthrough energies

To examine the behaviour of protons, they were simulated with different energies traversing through cylinders of varying length and the results can be seen in Figure 20.

Since it is helpful to visualize how the punchthrough energy varies with traversed length, the energies where punchthrough first occur is plotted against the length of the crystal, see Figure 21.

5 Results

5.1 Horizontal scintillators

5.1.1 Variations in area

Results from simulations with differently sized scintillators are shown In Figure 22 and Table 4.

The data show that the variation in size hardly affects the values of MPV or σ, but that it has a significant effect on the number of muons that pass through both scintillators in a given timespan.

5.1.2 Muon particle flux

The limiting factor for the calibration detector is the number of muons that pass the horizontal setup in the time allowed. The horizontal scintillator setup with the most favorable geometry has a total muon particle flux of $J_tot = 7.2788 \cdot 10^{-4}\,\mathrm{s}^{-1}$ i.e. one muon passes the two detectors

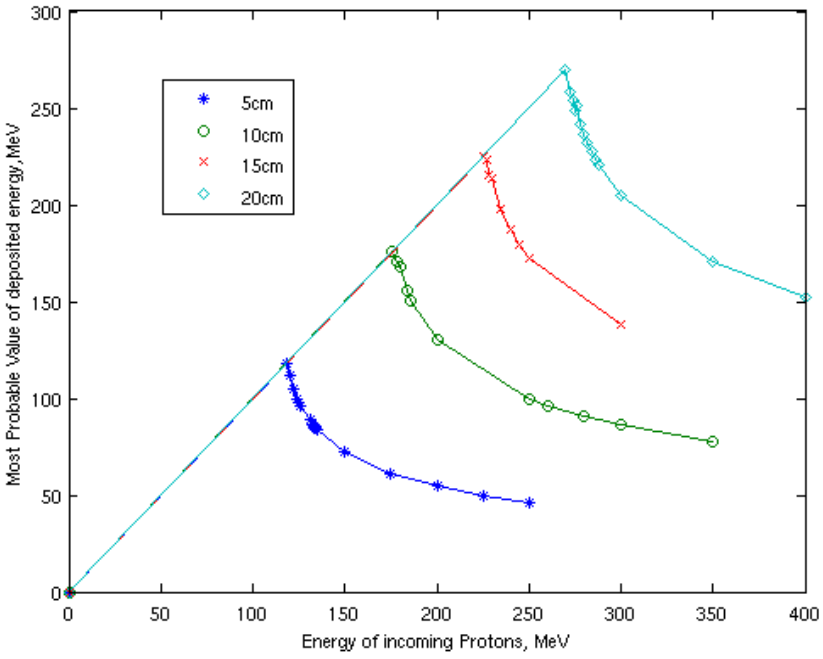

Figure 20: MPV from the Gaussian fits from simulations where protons with different energies are shot through NaI crystals of varying lengths, plotted against the incoming energy. The non-linear parts correspond to energies larger than the punchthrough energies. The plot contains error-bars (for the MPV-value) for energies above punchthrough energies which are not visible due to their small size.

side [cm]	n	MPV(σ) [MeV]	hits/10^6
5.5	1121	102.74(5.09)	22.4
9.5	1861	103.04(4.88)	62.0
13.5	11079	102.57(4.67)	123.1
17.5	10020	102.54(4.71)	200.4

Table 4: Results from simulations of horizontal muons for back scintillators with different side lengths. n is the registered number of particles, MPV and σ are the "most probable value" and its corresponding uncertainity from a Landau fit to the data. Hits/10^6 is the number of muons that took a path through both scintillators per one million simulated muons.

every 1374 seconds ($\tau = 1374\,\mathrm{s}$). See Table 5 for the time required for different number of muon hits in the horizontal scintillators.

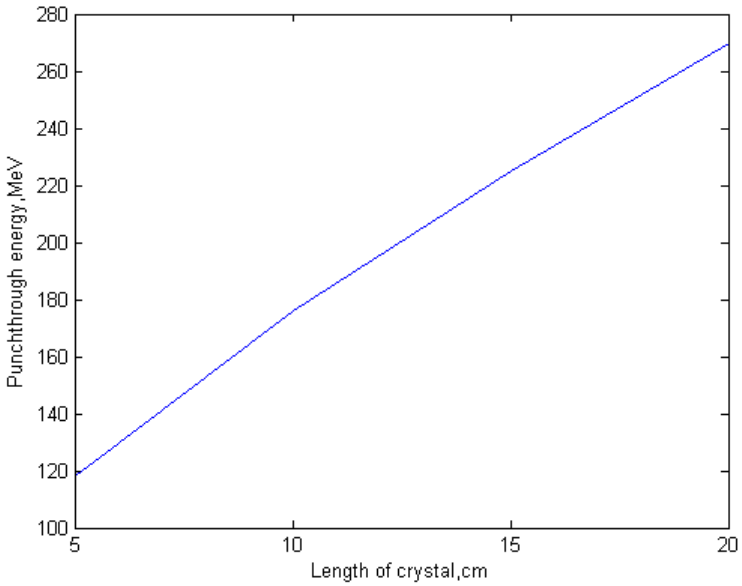

Figure 21: Punchthrough energies plotted against the length of the NaI crystal in which they are recorded. This figure does not contain error-bars.

Hits	Time [days]	σ (error(σ)) [MeV]
100	1.59	10.2651 ($\pm$3.64152)
200	3.18	6.14709 ($\pm$0.555548)
750	11.93	5.28359 ($\pm$0.231295)
1250	19.88	4.60752 ($\pm$1.68733)

Table 5: Estimated time required for calibration of the horizontal setup, for different numbers of muon hits in the horizontal setup, σ is the spread of a Landau fit to the data.

5.1.3 Variations in separation

Results from the simulations where scintillator separation was changed can be seen in Figure 23 and Table 6.

The data show that the variation in separation hardly has any effect on the values of MPV or σ, but that it has a significant effect on how many muons that pass through both scintillators in a given timespan.

5.2 Vertical scintillators

The scintillator setups can bee seen in Figure 24. The scintillators were placed above and below the crystal as in Figure 8, with a separation of 15 cm. The diagrams show the MPV and σ of a Landau fit to the amount of deposited energy in the crystal when a muon passed through two scintillators aligned on top of each other. Obtained values for min, max and mean of σ can be

(a) $5.5 \times 5.5\,\text{cm}$ (b) $9.5 \times 9.5\,\text{cm}$

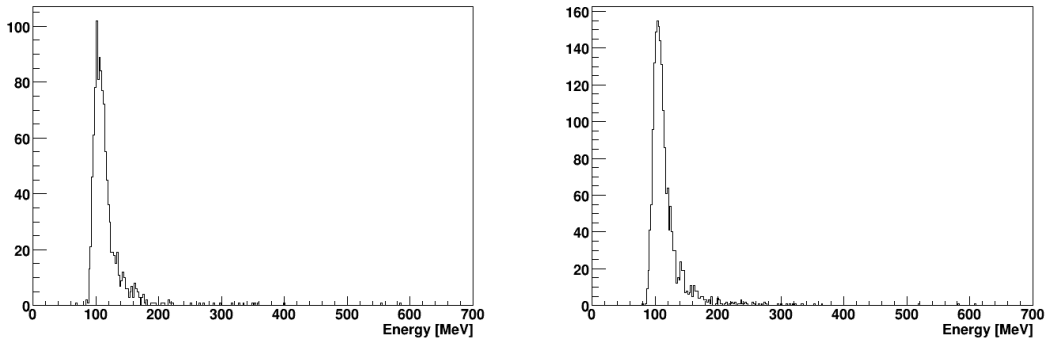

(c) $13.5 \times 13.5\,\text{cm}$ (d) $17.5 \times 17.5\,\text{cm}$

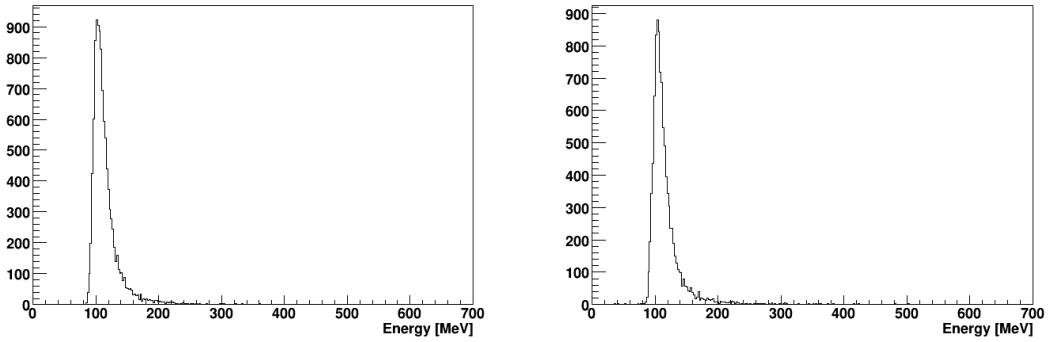

Figure 22: Histograms of energies deposited in the NaI crystal for horizontal square plastic scintillators of different side lengths.

separation [cm]	n	MPV(σ) [MeV]	hits/10^6
42	1330	102.42(4.70)	14.8
47	932	102.50(5.17)	11.7
52	732	102.02(4.98)	9.0
57	427	102.92(5.14)	7.12

Table 6: Results from simulations of horizontal muons for different plastic scintillator separations. n is the registered number of particles, MPV and σ are the "most probable value" and spread of a Landau fit to the data. Hits/10^6 is the number of muons that took a path through both scintillators per one million simulated.

found in Table 7.

The data show that, as the scintillators get smaller, the σ of the Landau fits get smaller, which corresponds to a narrower distribution of energy deposited in the crystal when a muon has travelled through two plastic scintillators placed vertically above each other. Data also shows

(a) 42 cm (b) 47 cm

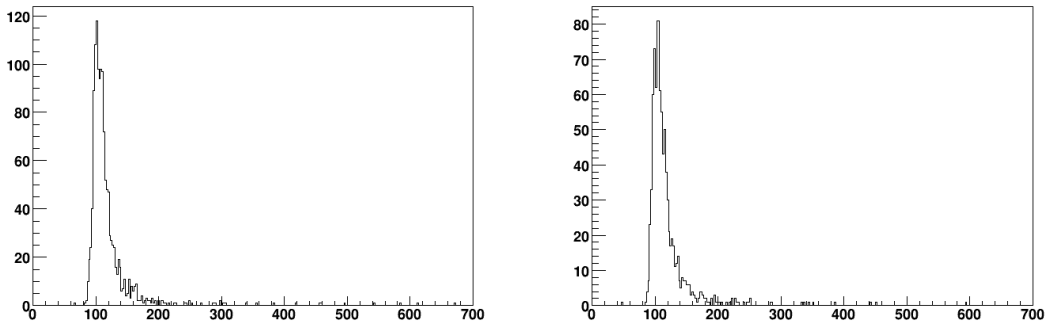

(c) 52 cm (d) 57 cm

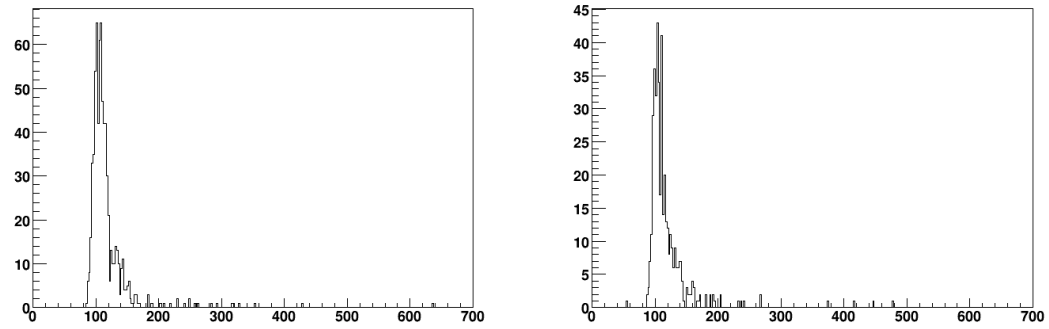

Figure 23: Histograms of energies deposited in the crystal for horizontal trajectory square scintillators of the same size, but with different separations.

Size	n	σ_{min}	σ_{mean}	σ_{max}
$10 \times 20\,\text{cm}$	1	4.13	4.13	4.13
$10 \times 10\,\text{cm}$	2	2.49	2.71	2.93
$6.67 \times 6.67\,\text{cm}$	3	1.96	2.41	2.72
$5 \times 5\,\text{cm}$	4	2.01	2.46	2.83
$4 \times 4\,\text{cm}$	5	1.91	2.39	2.87
$3.33 \times 3.33\,\text{cm}$	6	1.89	2.30	2.56
$2.86 \times 2.86\,\text{cm}$	7	1.78	2.40	2.83
$2.5 \times 2.5\,\text{cm}$	8	1.76	2.40	2.94

Table 7: Results from simulations of vertical scintillator setups. Data presented as scintillator sizes, number of crystals in a scintillator array together with minimum, mean and max values of σ from a Landau fit to the data.

that when when the scintillator size shrinks below (roughly) $5 \times 5\,\text{cm}$ the values of σ_{mean}-and σ_{max} do not decrease any more. The fact that σ_{min} still decreases with decreased scintillator size is probably due to surface effects: as the scintillators shrink in this simulation, the outermost ones get closer to the edges and thus measure trajectories that are close to a surface, where energy gets dissipated to the outside of the detector with high probability.

This implies that there is a limit where the broadening of the deposited energy due to the size of the scintillators is negligible, and the observed broadening can be traced to the statistical physical processes of particles interacting with matter, which introduces an uncertainty in how much energy is deposited. This also means that there is a limit beyond which it is not useful or necessary to shrink the scintillators.

6 Suggested experimental setup

We have studied two different types of setups for the calibration. One with ordinary scintillation counters and one with position sensitive scintillation counters. Since the latter is a lot more complicated to implement our suggestion is to try it only if there is enough time to change to the other setup, in case of failure.

6.1 Ordinary scintillation counter

The bottleneck in the process of measuring muons is the horizontal flux through the length of the crystal, given that the crystal should stay horizontal during the collection of data, and that the calibration should not take more time than three days.

The simulations above have showed that since the size of the back scintillator does not affect the MPV or σ, it would be preferable to maximize the areas of the horizontal scintillators, while making sure that the muons going through both scintillators traverse the whole length of the crystal. Considering the needed space for a PMT at the back end of the crystal, we suggest two square scintillators - $5 \times 5\,\text{cm}$ and $13.7 \times 13.7\,\text{cm}$, see Figure 25.

It was also shown that shrinking the square scintillators beyond $5 \times 5\,\text{cm}$ did not improve much on the error of the measurement, so we suggest using scintillators of this size. In order to minimize the impact of surface effects the scintillators should be placed at least 1 cm from edges (see 16). These things considered we would suggest a setup with three pairs of scintillators measuring $5 \times 5\,\text{cm}$ placed vertically above each other, 1 cm from the back edge of the crystal. The placement over the thicker end minimizes the relative difference between the longest and the shortest possible traversed path traversed through the crystal by the muons.

6.2 Position sensitive scintillation counter

One idea that we investigated is connecting four photomultiplier tubes (PMTs) to each scintillator, thereby making it possible to calculate where muons hit the scintillator in the following way.

The equation for a circle in a Cartesian coordinate system is

$$(x-a)^2 + (y-b)^2 = r^2 \tag{18}$$

where (a, b) is the center and r is the radius.

When a muon travels through the scintillator photons are emitted. Part of these photons are then detected by the PMTs. If the scintillator is thin, one can assume that it is two dimensional which means that the muon travels through it at a position (x_m,y_m), see Figure 6.2. From Figure 6.2 one sees that the connection points for the PMTs are located on circles centered at (x_m, y_m) and with radii r_0, $(R_1 + r_0)$, $(R_2 + r_0)$ and $(R_3 + r_0)$, respectively. To get R_1, R_2 and R_3 one multiplies the time difference one measure between each connection point and the connection point for the PMT which is first to detect photons. In reality one will have to know the time it takes for photons to travel between a connection point a PMT so one can substract that time from the actual measured time.

If one inserts the radius and position for the connection points into the equation for a circle (18) one gets four coupled equations (19).

$$\begin{cases} x_0^2 - 2x_0x_m + x_m^2 + y_0^2 - 2y_0y_m + y_m^2 = r_0^2 \\ x_i^2 - 2x_ix_m + x_m^2 + y_i^2 - 2y_iy_m + y_m^2 = r_0^2 + r_0R_i + R_i^2 \qquad i = 1,2,3 \end{cases} \tag{19}$$

Substitution of the first equation from the three others and some algebra results in a matrix equation (20).

$$\begin{bmatrix} 2x_0 - 2x_1 & 2y_0 - 2y_1 & -R_1 \\ 2x_0 - 2x_2 & 2y_0 - 2y_2 & -R_2 \\ 2x_0 - 2x_3 & 2y_0 - 2y_3 & -R_3 \end{bmatrix} \begin{bmatrix} x_m \\ y_m \\ r_0 \end{bmatrix} = \begin{bmatrix} x_0^2 - x_1^2 + y_0^2 - y_1^2 + R_1^2 \\ x_0^2 - x_2^2 + y_0^2 - y_2^2 + R_2^2 \\ x_0^2 - x_3^2 + y_0^2 - y_3^2 + R_3^2 \end{bmatrix} \tag{20}$$

Solving this system of equations gives (x_m, y_m) which is the point where the muon passed the scintillator.

7 Conclusions and Discussion

To calibrate a single crystal with the proton beam, we note that the beam has a well-defined energy and this energy should be such that it is below the punchthrough energy. This can be guaranteed thanks to the fact that the punchthrough energy varies linearly with length, see Figure 21. The path that the proton beam will take is 20 cm long and the proton energy should thus be less than 288 MeV.

This beam, which is monodirectional and monoenergetic, gives us a well-defined peak in the deposited energy corresponding to the incoming energy of the protons, see Figure 19. The resolution, being less than 2 % for protons being stopped in the crystal [20], will not affect the results. The energy deposited in the crystal by incoming protons will be known by correlating the signal resulting from muon interactions in the crystal and the deposited energy of the protons.

From the simulations in Section 4.1.1 one sees that muons in this energy-range do indeed behave as minimum ionizing particles. As such, the deposited energy should not depend on the incoming energy of the muons, which is supported by our simulations, see Figure 14. One can thus use muons to calibrate the Crystal Ball. Their path through the ball is known because single muons will make different crystals fire and the path can be calculated. The signal resulting from the energy deposit can hence be calibrated.

An issue that arise for protons that are not stopped by Crystal Ball is that their energy can not be determined unambiguously, by being mistaken as lower energy stopped ones, see Figure 20.

One thing that should be considered in further studies and simulations is how the thickness of the plastic scintillators affects the processes. This study only considered square plastic scintillators with a fixed thickness of 0.5 cm. It would be of interest to run more simulations with other shapes and thicknesses to further investigate parameters that would contribute to making good measurements. Geant4 has many possibilities to easily simulate physical bodies of many different geometrical shapes, and plastic can be manufactured into many different shapes, so the realizable variations are endless in simulation and in the lab.

Simulations were time consuming with the computer power available to the group. The simulation time required to get a decent amount of muons through both scintillators in the horizontal setups could take up to 10 hours for small scintilator sizes. One should look into possibilities to optimize code, especially the muon distribution, to speed up simulations, and make time available for testing more scintillator setups and properties.

There has been some indications that the theoretical muon distribution might have a too low intensity. Researchers have found that experiments yielded a double muon flux compared to simulations using the same data as this study[21]. This is promising, as this would cut down calibration time.

(a) $10 \times 20\,\text{cm}$

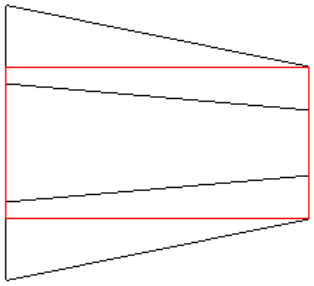

(b) Deposited energy

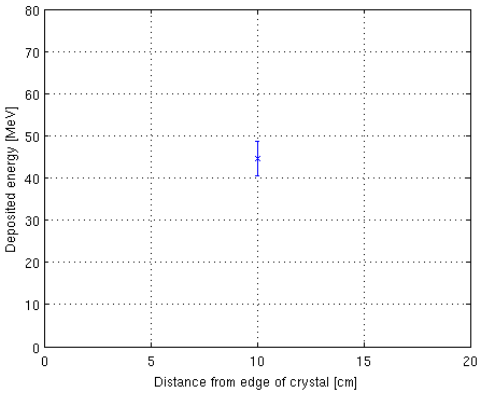

(c) $6.67 \times 6.67\,\text{cm}$

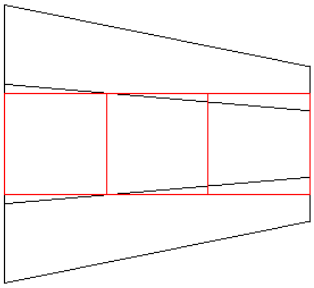

(d) Deposited energy

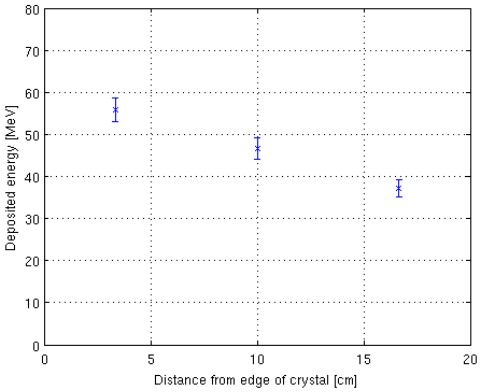

(e) $2.86 \times 2.86\,\text{cm}$

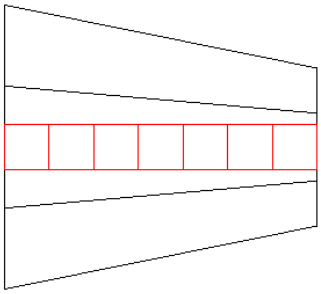

(f) Deposited energy

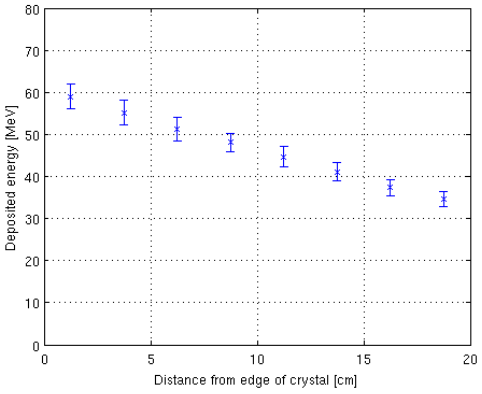

Figure 24: Scintillator sizes and setups with corresponding deposited energies. The crosses and error bars represent MPV and σ from a curve fit to a Landau distribution. The x-coordinates in the plots show distance from the thick end of the crystal to the center of a scintillator.

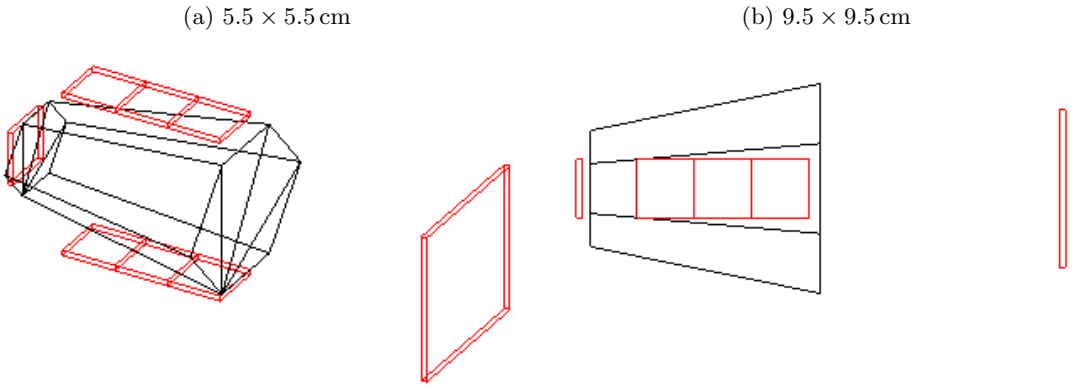

Figure 25: Scintillator setup to maximize horizontal muon flux, avoid surface effects, and gather accurate data with plastic scintillators.

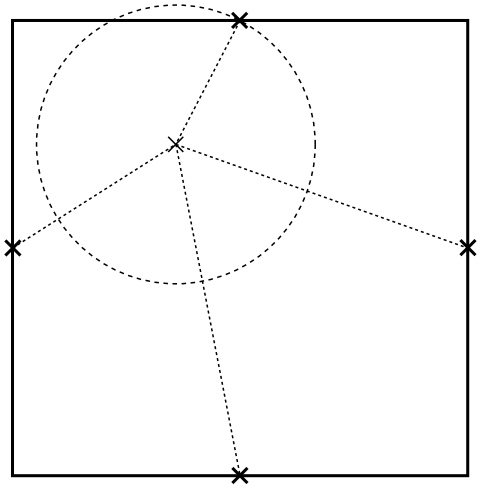

Figure 26: An example of a muon passing the position sensitive scintillator at (x_m,y_m).

References

[1] Adrich, P. (2003) *The Crystal Ball γ-Detector Setup and Calibration.* Retrieved 8 February, 2012, from GSI Helmholtzzentrum für Schwerionenforschung GmbH.
`http://www.gsi.de/forschung/kp/kp2/collaborations/land/doc/detectors/crystal_ball/cb_docu.pdf`

[2] Geant4 collaboration, Agostinelli, S. et al. (2003). Geant 4 - a simulation toolkit, *Nuclear Instrument and Methods in Physics Research A*, vol. 506, pp. 250-303.

[3] Geant4 collaboration, Allison, J. et al. (2006). Geant4 developments and applications, *IEEE Transactions on Nuclear Science*, vol. 53, pp. 270-278.

[4] Amako, K. et al. (2005). Comparison of Geant4 electromagnetic physics models against the NIST reference data, *IEE Transactions on Nuclear Science*, vol. 52, pp. 910-918.

[5] Cirrone, G.A.P. et al. (2004). Precision validation of Geant4 electromagnetic physics, *i Conf. Rec. 2003 IEEE Nuclear Science Symposium*, vol. N23-2.

[6] Leo, W. R., (1994) *Techniques for Nuclear and Particle Physics Experiments.* Second revised edition. Berlin Heidelberg: Springer-Verlag.

[7] Devons, s et al. (1960). *Muon Mass and Charge by Critical Absorption of Mesonic X Rays.* Retrieved 15 May, 2012, from Columbia University.
`http://prl.aps.org/pdf/PRL/v5/i7/p330_1`

[8] Green, D. (2000). Ionization. In *The Physics of Particle Detectors*, red. D. Green, ss. 107-108. Cambridge: Cambridge University Press.

[9] Groom, D E. Klein, S R. (1999). *Passage of particles through matter.* Retrieved 10 May, 2012, from Lawrence Berkeley National Laboratory.
`http://www.springerlink.com/content/m321677145684107/fulltext.pdf`

[10] Groom, D E. Mokhov, N V. Striganov, S I. (2001) Muon Stopping Power and Range Tables 10 MeV-100 MeV. *Atomic Data and Nuclear Data Tables*, vol. 76, nr 2, pp. 183-356.
`http://pdg.lbl.gov/2008/AtomicNuclearProperties/adndt.pdf`

[11] Private communication with Heinz, A M. 15 May, 2012, from Chalmers University of Technology.

[12] Kempa, J. Brancus, M. (2003). Zenith angle distributions of cosmic ray muons. *Nuclear Physics B (Proc. Suppl.)*, vol. 122, pp. 279-281.

[13] Kempa, J. Krawczynska, A. (2006). *Low energy muons in the cosmic radiation*. Retrieved 13 Mars, 2012, from Warzaw University of Technology.

[14] Liu, L. (2007). *The Speed and Lifetime of Cosmic Ray Muons*. Retrieved 15 May, 2012, from Massachusetts Institute of Technology.
`http://web.mit.edu/lululiu/Public/pixx/not-pixx/muons.pdf`

[15] National University of La Plata. (n. d.). *Muon basics*. Retrieved 8 February, 2012, from National University of La Plata.
`http://www.fisica.unlp.edu.ar/~veiga/experiments.html`

[16] Nilsson, T. (2011). *ROOT analysis, simple simulation and curve fitting write-up for the course "FUF065/FIM465 Advanced Subatomic Detection and Analysis Methods"*. Retrieved 9 February, 2012, from Chalmers University of Technology.
`http://fy.chalmers.se/subatom/advsubdet/ROOT_small.pdf`

[17] Official website of the Geant4 collaboration. (n. d.). *Geant4: A toolkit for the simulation of the passage of particles through matter*. Retrieved 9 February, 2012, from
`http://geant4.org/`

[18] *ROOT*, Retrieved 15 May, 2012, from `http://root.cern.ch/`

[19] Saint-Gobain Ceramics & Plastics Inc. (2005). *BC-400, BC-404, BC-408, BC-412, BC-416 Premium Plastic Scintillators Datasheet*.

[20] Wamers, F. (2011). *Quasi-Free-Scattering and One-Proton-Removal Reactions with the Proton-Dripline Nucleus* ^{17}*Ne at Relativistic Beam Energies*, Technische Universität Darmstadt, pp. 31-32.

[21] Private communication with Thies, R. 15 May, 2012, from Chalmers University of Technology.